Materials Science inc. Nanomaterials & Polymers

Fabrication and Evaluation of Flexible Micro-Supercapacitor from MWCNTs-Ag Nanohybrid-Sulfonated PANI Nanocomposite Embedded PVA-TEOS Membrane

Satishkumar R. Naik, Anand I. Torvi, Balappa B. Munavalli, Divya D. Achari, and Mahadevappa Y. Kariduraganavar*[a]

The flexible nanocomposite membranes were developed by incorporating the multiwalled carbon nanotubes-silver nanoparticle-sulfonated polyaniline (MWCNTs–Ag-SPANI) nanocomposite in TEOS crosslinked PVA matrix. The physicochemical properties of the resulting ternary nanocomposite membranes were investigated systematically by different techniques. The electrochemical performance of all the nanocomposites was evaluated by cyclic voltammetry, galvanostatic charge-discharge and electrochemical impedance spectroscopy. The nanocomposite containing 1:1 weight ratios exhibited a maximum specific capacitance of 572.8 $F g^{-1}$ with energy density of 79.5 $Wh kg^{-1}$ and power density of 9.9 $kW kg^{-1}$. A remarkable electrochemical performance of ternary nanocomposite was associated due to the synergistic effect of MWCNTs, SPANI and Ag nanoparticles. Around 83.5% capacitance retention was found even after 2500 cycles, revealing that nanocomposite exhibited an excellent stability. Considering these superior performances, a micro-supercapacitor device was fabricated from the developed nanocomposite membrane and evaluated its electrochemical performance. The fabricated micro-supercapacitor device showed specific capacitance of 60.95 $F g^{-1}$, energy density of 7.46 $Wh kg^{-1}$ and power density of 67.81 $W kg^{-1}$ at a current density of 5.0 $mA g^{-1}$. Furthermore, the fabrication method adopted here could be easily applied to large-scale fabrication of flexible light-weight micro-supercapacitor devices.

Introduction

Today, energy storage has become a demanding task to the scientific society in response to the reduction of fossil fuel energy and global warming problems.[1–3] The development of handy electronic devices and hybrid electric vehicles with high energy density and power density are needed urgently.

Supercapacitors, also called electrochemical capacitors, have become one of the most promising candidates for next-generation energy storage devices because of their desirable properties including high power density, fast charging, excellent cycle-life stability and easy operational mechanism.[4–7] Great efforts have been made toward the fabrication of flexible supercapacitor devices considering their applications including portable electronics, digital communications, hybrid electric vehicles, etc.[8–14] Much research on supercapacitors is now focusing on cost-effective fabrication methods by the use of eco-friendly materials.[15–18] Among all the potential materials, carbon nanotubes (CNTs) have been widely studied considering their promising electric properties owing to their nano-scale texture, high surface area and low cost.[19–24] The surface modification of CNTs by conducting polymers has been exploited by the researchers due to their relatively lower specific capacitance and poor energy density issue.

Recently, many researchers have been focusing on the syntheses of binary and ternary composites of CNTs and conducting polymers to utilise their advantages in energy storage applications. Considering the reversible doping-dedoping chemistry and the stable electrical conduction mechanisms of polyaniline (PANI), researchers have been well explored the PANI composites containing multiwalled carbon nanotubes (MWCNTs) and single-walled carbon nanotubes (SWCNTs) for supercapacitors. For example, Meng et al.[25] reported paper-like CNT/PANI composite electrodes with good electrochemical properties. Otrokhov et al.[26] reported the enzymatic synthesis of polyaniline and MWCNTs, that exhibited the specific capacitance of 440 $F g^{-1}$. Similarly, the composites of sulfonated multiwalled carbon nanotubes and modified PANI nanorods (PANI/sMWCNTs) with maximum specific capacitance of 515.2 $F g^{-1}$ were developed by Zhu et al.[28]

Though the developed CNT based nanocomposites exhibit good specific capacitance, the flexibility of the electrode material is the essential factor for the fabrication of supercapacitor device. Incorporation of nanocomposite in the flexible polymer membrane could be an effective way to achieve this criterion. In order to obtain the membrane with homogenous dispersion of the nanocomposite, it is required to synthesize the composite with good solubility in common solvents such as water. Though PANI is a good electrochemical material, the solubility of PANI in aqueous media is a major drawback. The sulfonation of PANI by treating with chlorosul-

[a] Dr. S. R. Naik, Dr. A. I. Torvi, Dr. B. B. Munavalli, Dr. D. D. Achari, Prof. M. Y. Kariduraganavar
Department of Chemistry, Karnatak University, Dharwad-580 003, India
E-mail: mahadevappayk@gmail.com
kariduraganavarmy@kud.ac.in

Supporting information for this article is available on the WWW under https://doi.org/10.1002/slct.202003223

fonic acid in an inert solvent is one of the efficient methods to improve the solubility of PANI in aqueous media. However, the presence of strong electron-withdrawing sulfonic acid (–SO_3H) groups significantly reduces the conductivity of sulfonated polyaniline (SPANI) as compared to pure PANI. The electrical conductivity of the water-soluble SPANI could be improved by introducing the silver (Ag) nanoparticles. Thus, it is clear that the development of CNT–Ag-SPANI ternary nanocomposites would fulfil the major requirements for the development of flexible membrane electrode.

There are reports on PANI–Ag, CNT–Ag and Ag-PANI-CNT nanocomposites in the literature.[29–33] However, the synthesis of ternary nanocomposites based on sulfonated polyaniline, multiwalled carbon nanotube and silver nanoparticles is not yet reported. Also, to the best of our knowledge, there are no reports available on the development of flexible electrode material by the incorporation of ternary nanocomposite in the polymer matrix.

Understanding this, we have synthesized MWCNTs–Ag-SPANI ternary nanocomposite and incorporated into the PVA matrix to develop the flexible and electrochemically active nanocomposite membrane. Initially, PANI was synthesized using ammonium persulfate (APS) as an oxidant for the polymerization of aniline monomer and functionalized with sulfonate groups to obtain SPANI. Later, the MWCNTs–Ag binary nanocomposite was synthesized by depositing the silver nanoparticles on the surface of the MWCNTs via wet chemical process. Consequently, MWCNTs–Ag-SPANI ternary nanocomposite was synthesized and incorporated into the PVA matrix and subsequently crosslinked with tetraethyl orthosilicate (TEOS). The schematic representation of MWCNTs–Ag-SPANI ternary nanocomposite incorporated PVA-TEOS membrane is shown in Figure 1. The synthesized ternary nanocomposite was water-soluble and thus it was explored to develop homogenous polymer electrode material. The synthesized ternary nanocomposite has drawn a significant attention as it combines the pseudocapacitance behavior of SPANI, Ag nanoparticles and the electrical double layer characteristics of MWCNTs. The resulting electrode material was optimized by tuning the weight ratio of MWCNTs–Ag nanohybrid and sulfonated polyaniline in the polymer matrix. The developed nanocomposite membrane electrodes were systematically investigated to explore their application in supercapacitors.

Based on the superior electrochemical performance exhibited by the developed ternary nanocomposite membrane, we have fabricated the micro-supercapacitor device and evaluated the electrochemical performance in terms of specific capacitance, power density, energy density, etc. The schematic representation for the fabrication of the micro-supercapacitor device is shown in Figure 2a. The bendings of the fabricated device at different angles such as 0, 90 and 180 degrees are shown in Figures 2b, 2c and 2d, respectively. This showed an excellent flexibility of the fabricated device. The obtained results were discussed based on the design employed for the fabrication of micro-supercapacitor device and the properties of the material. The results clearly suggest that the fabricated

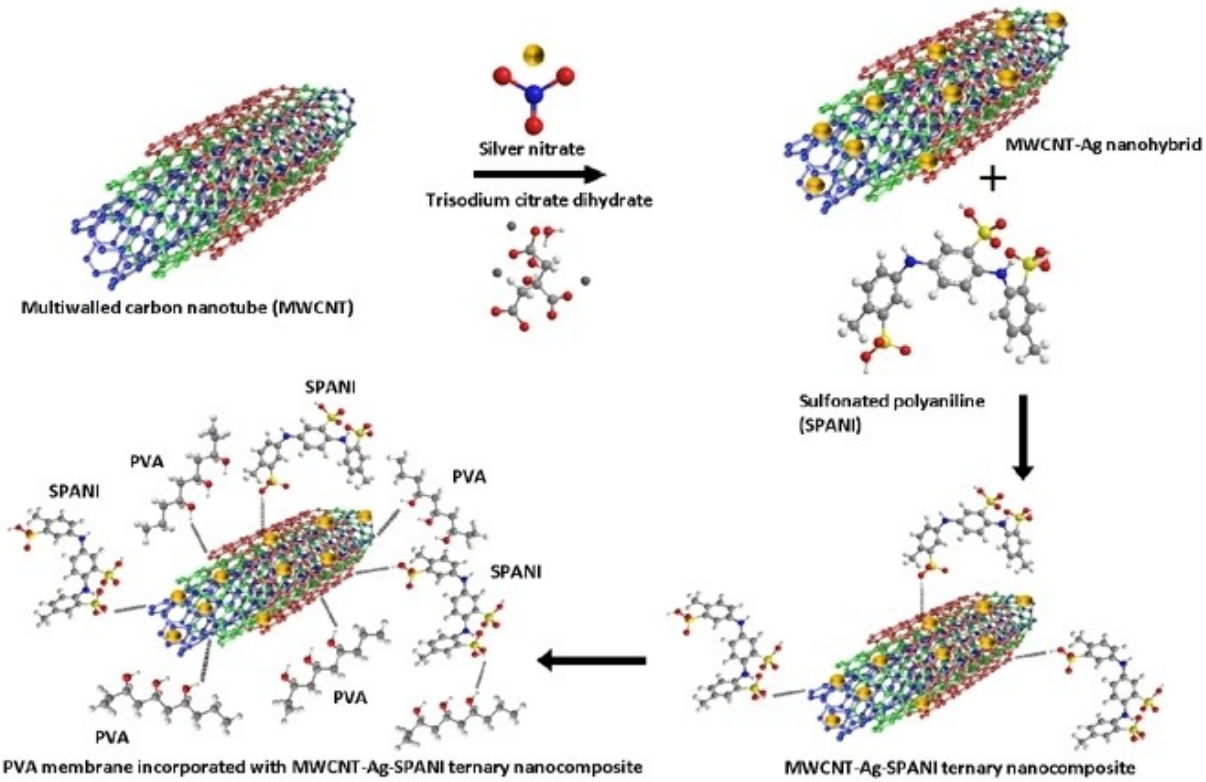

Figure 1. The schematic representation of the preparation of PVA-TEOS membrane incorporated with MWCNTs–Ag-SPANI.

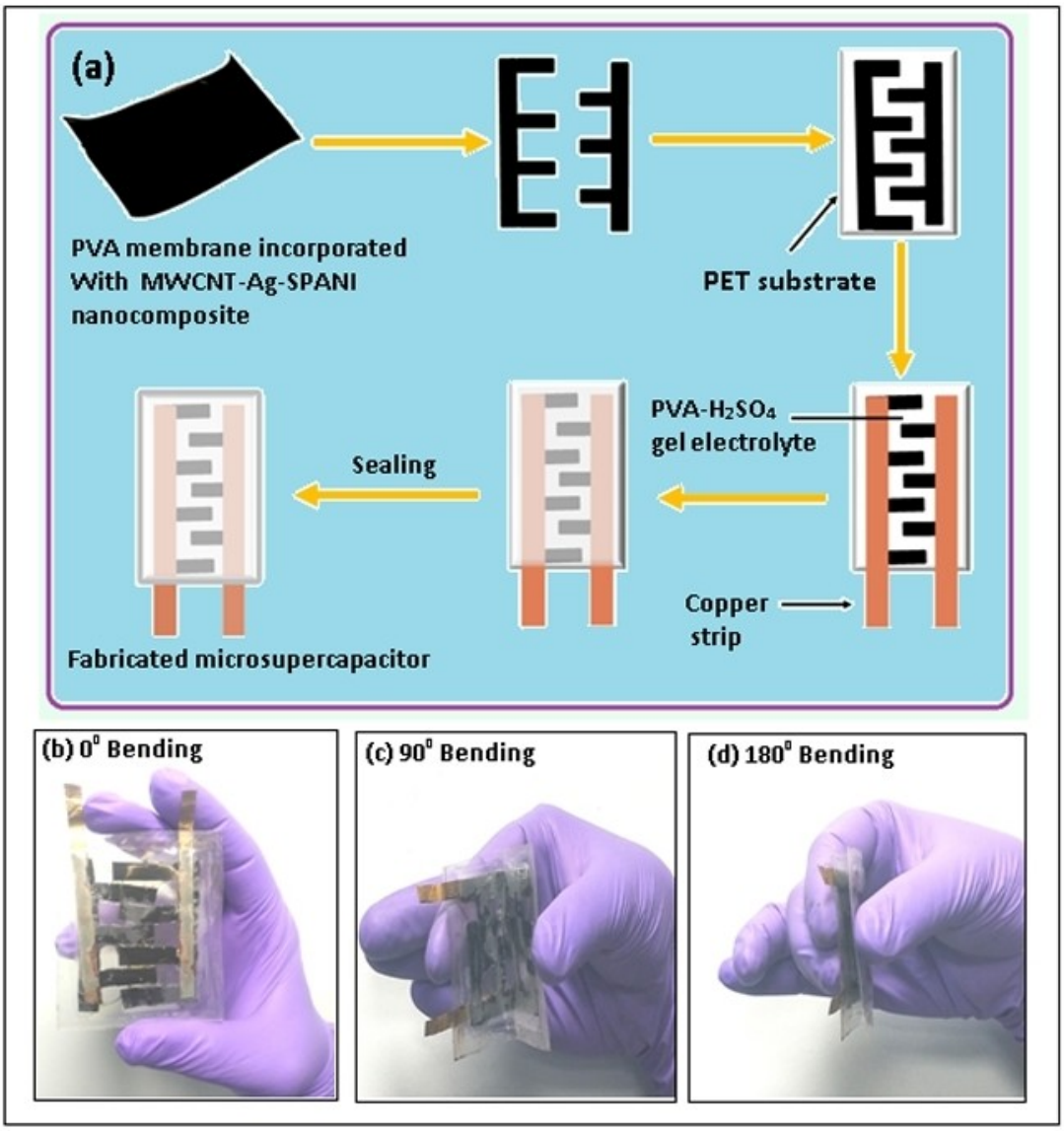

Figure 2. (a) The schematic representation for the fabrication of micro-supercapacitor, (b, c and d) the bendings of the fabricated micro-supercapacitor device at 0, 90 and 180 degrees.

micro-supercapacitor device could be a potential candidate for flexible electronics applications.

Results and discussion

Fourier transform infrared (FT-IR) spectroscopy was employed to investigate the structure and functional groups present in MWCNTs, SPANI, MWCNTs–Ag, MWCNTs–Ag-SPANI and PMWAgP nanocomposite, and the resulting spectra are presented in Figure 3. A broad band observed at around 3440 cm^{-1} in the spectrum of MWCNTs was assigned to the –OH stretching vibration. The spectrum has stretching vibration near 1630 cm^{-1} and is due to the presence of a carbonyl (C=O) group that was formed by the acid treatment. The band appeared at around 1560 cm^{-1} corresponded to C=C stretching vibrations. Similarly, the bands present at around 2925 and 2856 cm^{-1} were assigned to -CH_2 stretching vibrations. The band appeared at 526 cm^{-1} in the spectrum of MWCNTs–Ag composite is due to the Ag–C stretching vibration. In the spectrum of SPANI, the characteristic stretching bands observed at 1565 and 1485 cm^{-1} are due to the stretching vibrations of the quinoid ring and benzenoid ring, respectively.[33] These bands indicate the formation of emeraldine salt state of PANI and the pi-pi interaction between the rings of PANI and graphitic structure of CNT. Similarly, in the spectrum of PMWAgP, the bands observed at 1300 and 1240 cm^{-1} are assigned to C–N stretching and C=N stretching, respectively. The broad bands appeared in the region of 1000–1100 cm^{-1} are attributed to the formation of Si–O–C bonds between linear alkyl chain (–CH_2–CH–) of PVA.[34] The band

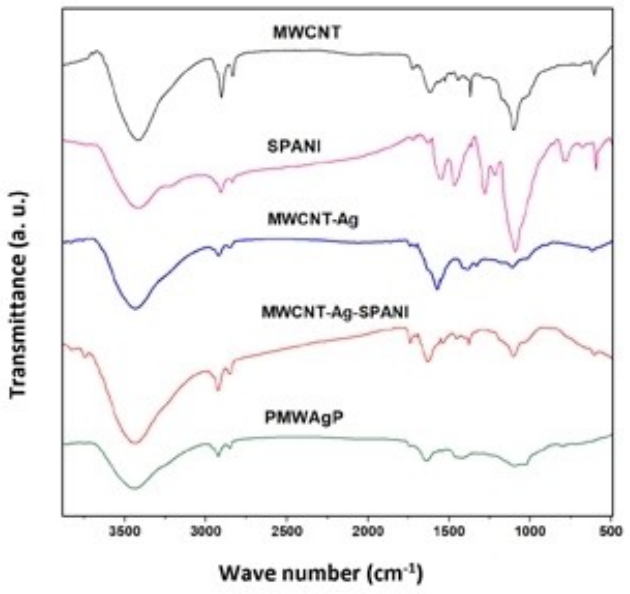

Figure 3. The FTIR spectra of MWCNTs, SPANI, MWCNTs–Ag, MWCNTs–Ag-SPANI and PMWAgP nanocomposite.

appeared at 1240 cm^{-1} is the confirmatory band of SPANI for its conductivity.

The crystallinity of developed SPANI, MWCNTs–Ag and MWCNTs–Ag-SPANI (MWAgP) nanocomposite was confirmed by powder X-ray diffraction (PXRD) analysis between 10 and 100°, and the PXRD patterns are displayed in Figure 4. The PXRD spectra clearly indicate a peak at 26.31° which resembles

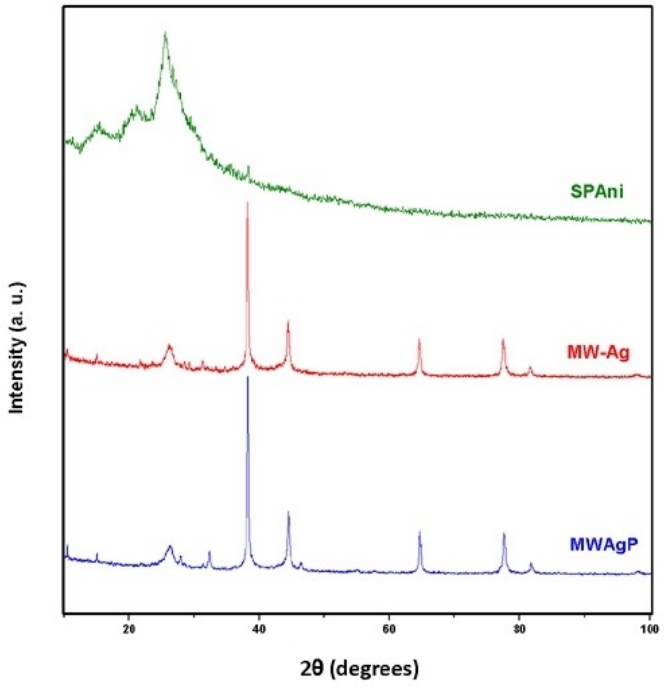

Figure 4. PXRD patterns of SPANI, MW–Ag and MWAgP nanocomposite.

the (002) plane of CNTs.[35,36] The sulfonated PANI exhibited peaks at $2\theta = 14.99$, 20.66° and 25.35°, which are corresponded to the periodicity parallel and perpendicular to the polymer chains, respectively.[37,38] The MWCNTs–Ag binary composite exhibited peaks at 2θ values of 38.19, 64.52 and 77.42, which are respectively corresponded to the (111), (220) and (311) planes, and this is very well supported by the literature.[39–41] The PXRD results also suggest that MW–Ag and MWAgP nanocomposites are more crystalline than that of sulfonated PANI and this could be due to the presence of crystalline Ag nanoparticles.

The thermal stability of all the developed PMWAgP nanocomposites was studied by thermogravimetric analysis (TGA), and the thermograms are displayed in Figure 5. All the thermograms of PMWAgP nanocomposites are almost matching with each other, which may be due to the low content of reinforcement of constituents. In all the thermograms, the initial weight loss detected from ambient to 100 °C was ascribed to the removal of moisture.[42] A slight weight loss of around 5–10% was corresponded to the decomposition of the thermally unstable organic functional moieties present in the nanocomposites. The major weight loss of about 30% from ~230 °C to ~350 °C was ascribed to the decomposition of sulfonated PANI and PVA side chain present in the nanocomposite. The weight loss observed from ~350 °C to ~450 °C was attributed to the decomposition of PVA main chain, and beyond this temperature, MWCNTs will start to undergo degradation. At 300 °C, only 25.8% weight loss occurred for PMWAgP-3 nanocomposite, while 35.5, 32.7, 29.6 and 28.3% degradation occurred for PMWAgP-1, PMWAgP-2, PMWAgP-4 and PMWAP-5, respectively. This trend suggests the superior thermal stability of PMWAgP-3 nanocomposite membrane owing to the presence of stronger interaction between MWCNTs and PANI layer at the optimised ratio. Some residual weight observed at around 600 °C and this was attributed to the undecomposed silver content present in the nanocomposite. The increased residual weight contents of 22, 24, 31, 33, and 36% for five nanocomposite membranes namely, PMWAgP-1, PMWAgP-2, PMWAgP-3, PMWAgP-4 and PMWAgP-5, respectively was in accordance with the weight ratio of MW–Ag and SPANI.

The thermal behaviour of all the nanocomposites was also investigated by differential scanning calorimetry (DSC). The DSC thermograms presented in Figure 6 shows an endothermic peak at 70–120 °C, which corresponded to the vaporisation of moisture content entrapped in the polymer backbone. The exothermic peak at 150–220 °C is associated with the subsequent bond scissoning and bond formation of MWCNTs-PANI composites by the formation of free radicals.[43] From the thermograms it is also observed that the melting temperature (T_m) increased with increasing the MWCNTs–Ag nanohybrid up to the weight ratio 1:1 (PMWAgP-3). This could be due to the increased ionic interaction between the sulfonic groups of SPANI and the carboxyl groups of MWCNTs. With increasing the crosslinking density, the melting temperatures of the resulting membranes were increased as expected. On the contrary, in case of PMWAgP-4 and PMWAgP-5, the melting temperature did not show any significant changes and this is

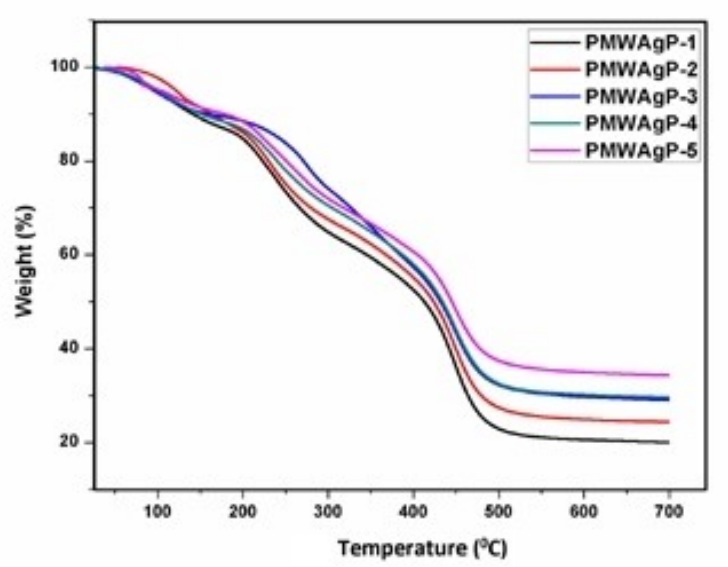

Figure 5. TGA thermograms of PMWAgP nanocomposites.

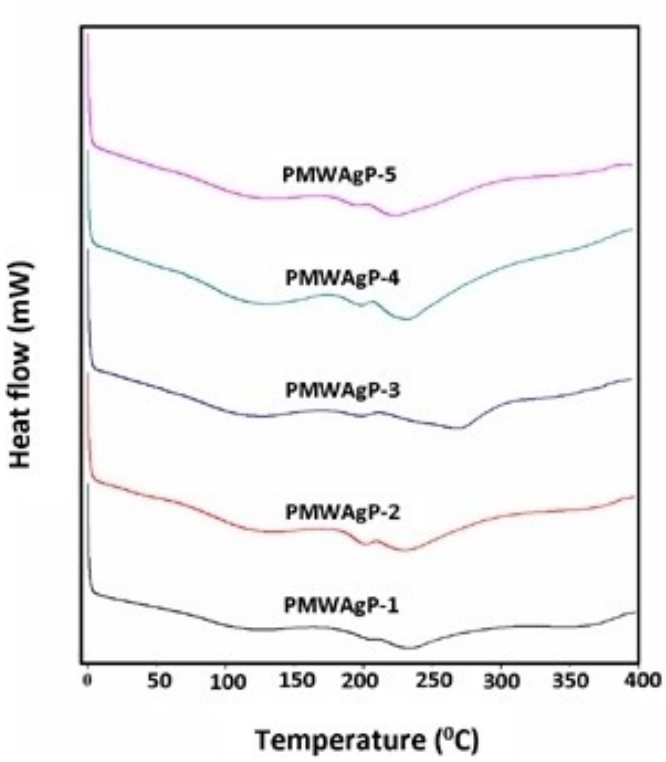

Figure 6. DSC patterns of PMWAgP nanocomposites.

due to the hindrance caused by the excess amount of MWCNTs and Ag nanoparticles. All these results clearly reveal that PMWAgP-3 exhibited a good thermal stability.

The contact angle measurement was carried out to know the hydrophilic nature of the developed nanocomposite membranes as it enhances the electrochemical performance of membrane-based electrodes. Several factors, such as pore size, membrane roughness and the pore size distribution may have an impact on the hydrophilicity. Higher the hydrophilic nature lower is the contact angle. The water contact angles obtained from the measurement are 68.5°, 67.1°, 65.6°, 56.5° and 50.3°, respectively for PMWAgP-1, PMWAgP-2, PMWAgP-3, PMWAgP-4 and PMWAgP-5 nanocomposites, which are presented in Figure S2 in supporting information. The contact angle less than 90° indicates that all the nanocomposite membranes were hydrophilic in nature, and it helps for the intimate contact of electrolyte ions with the electrode material. A noticeable gradual decrease in contact angle observed for the five nanocomposite membranes was associated with the incremental increase in the content of multiwalled carbon nanotube-silver nanohybrid (MW–Ag) with respect to sulfonated polyaniline (SPANI) in the nanocomposites. The increased hydrophilicity with increasing the mass loading of MW–Ag is due to the spontaneous migration of well-dispersed MW–Ag nanohybrid on the surface of sulfonated PANI at the membrane-water interface, which imparts superior hydrophilicity by reducing the interfacial energy.[44] The hydrophilic nature of nanocomposite facilitates easy intercalation or deintercalation of H^+ ions of aqueous electrolyte to or from the electrode and thus enhances the ionic conductivity. The contact angle results are in good agreement with the electrochemical performance. The influence of the ternary nanocomposite on the mechanical properties of the developed membranes was tested with a universal testing machine. The results are summarized in Table 1. From the data, it is clear that the tensile strength and Young's modulus of the samples decreased with increasing the MW–Ag nanohybrid content in the ternary nanocomposite. This decreased behaviour might be associated with the weakened inter-and intra-molecular hydrogen bonding estab-

Table 1. The mechanical stability data of PMWAgP nanocomposites.[a]

Sl. No.	Polymer Composite	Tensile Strength [MPa]	Elongation at Break [%]	Young's Modulus [MPa]
1	PMWAgP-1	59.733	19.755	2300.814
2	PMWAgP-2	53.945	19.315	1777.176
3	PMWAgP-3	52.909	15.932	1315.779
4	PMWAgP-4	45.641	13.442	812.194
5	PMWAgP-5	40.864	13.392	719.458

[a] The synthesis is described in Figure 1.

lished inside PVA matrix upon the introduction of the ternary nanocomposite.

Among the ternary nanocomposite developed, PMWAgP-3 displayed relatively good mechanical stability with a tensile strength of 52.909 MPa, Young's modulus of 1315.779 MPa and elongation at break of 19.755 %. This is due to the strong interaction occurred between ternary nanocomposite and the PVA. It is obvious that the nanocomposite membranes, combine with an excellent mechanical stability of PVA membrane and conductive behavior of MWAgP ternary nanocomposite, become a promising electrode material for the device application.

The surface morphology of the developed nanocomposites was analyzed by scanning electron microscopy (SEM) to understand the distribution of conducting PANI and silver nanoparticles on the surface of MWCNTs. The SEM images of five PMWAgP nanocomposites are shown in Figure 7. The SEM images show that the Ag nanocrystals grew on the surface of MWCNTs and were then covered within the anchored sulfonated PANI layers. The formation mechanism of MWAgP ternary nanocomposite may include the covalent interaction between MWCNTs and PANI and the strong electrostatic interaction between MWCNTs and Ag nanocrystals. It can be witnessed that the MWCNTs are well dispersed in the polymer matrix, and the interconnected nanosheets formed a conductive network and these overlap with each other throughout the length of the nanosheets. Besides, the nanotubes prevent the agglomeration of polyaniline layers and also form a composite with a porous architecture. This facilitates the transport of ions in the inner region of the electrode and finally led to the enhanced electrochemical performance of the material. From the SEM images, it is also observed that the agglomeration of MWCNTs increased with increasing the MW–Ag content in the composites, as shown in Figure 7d and 7e. This would lead to restacking of MWCNTs and thus restricts the electron flow.

To check the intercalation and deintercalation of the electrolyte in the developed electrode material, the degree of membrane swelling was performed in 1 M H_2SO_4 aqueous solution. The weights of the dry membranes were determined and then soaked in 1 M H_2SO_4 aqueous solution in a sealed vessel at 25 °C for different time intervals from 1 h to 12 h. After careful blotting, the swollen membranes were weighed immediately on a digital microbalance (Mettler, B204-S, Toledo, Switzerland). The same experiments were performed at least three times, and the average readings were taken. The percent degree of swelling (*DS*) was calculated from the Equation (1):

$$DS\ (\%) = \frac{W_{wet} - W_{dry}}{W_{dry}} \times 100 \quad (1)$$

where, W_{wet} and W_{dry} are the weights of wet membrane and dry membrane, respectively.

Sorption properties of the membrane play an important role in membrane-based electrochemical applications. Figure S3 given in supporting information shows the swelling behavior of all the five developed electrode materials performed at ambient temperature. From the data, it is clear that the degree of swelling was remarkably increased for all the samples with increasing the duration of time. This is due to increased interaction between an aqueous solution of H_2SO_4 and the membrane owing to the presence of interactive hydrophilic groups, like OH^- and H^+. This is a clear evidence for the easy penetrability of the electrolyte throughout the electrode material.

Electrochemical performances of the nanocomposite membranes

Cyclic voltammetry (CV), galvanostatic charge-discharge (GCD) and electrochemical impedance spectroscopy (EIS) studies were performed to ascertain the electrochemical performance of the developed nanocomposite membrane in a two-electrode system using 1 M H_2SO_4 aqueous solution as electrolyte. The CV curves recorded over a potential window of −1 V to +1 V at different scan rates from 2 mV s^{-1} to 100 mV s^{-1} are presented in Figure 8 (a–e). All the CV curves shows quasi-rectangular shape with redox current peaks, suggesting that the developed nanocomposite exhibited both the pseudocapacitive and EDLCs characteristics.[45] The CV curves of all the nanocomposites almost unchanged even up to 100 mV s^{-1}, suggesting a stable electrochemical performance of the samples even with the variation of scan rates.

For all the nanocomposites, the voltammograms showed a little shift in both anodic and cathodic peak potentials at all the scan rates, indicating a fast electrolyte transport and the electron transfer. It is also observed that both anodic and cathodic peak currents are proportional to scan rate, and this clearly suggests that the electrochemical reaction is a capacitive process. Figure 9a shows the cyclic voltammograms of all the nanocomposite samples recorded at a fixed scan rate of 50 mV s^{-1} between the potential window of −1.0 V and +1.0 V. A significant enhancement in the current response for PMWAgP-3 nanocomposite was observed, signifying that the developed PMWAgP-3 nanocomposite demonstrated an excellent electrochemical performance. This is mainly due to the synergistic effect of MWCNTs, Ag and SPANI. The CV curves show two sets of distinct redox anodic and cathodic current peaks owing to the presence of SPANI. The first set of redox peak is attributed to the conversion of the fully reduced leucoemeraldine base to the partially oxidized emeraldine. In

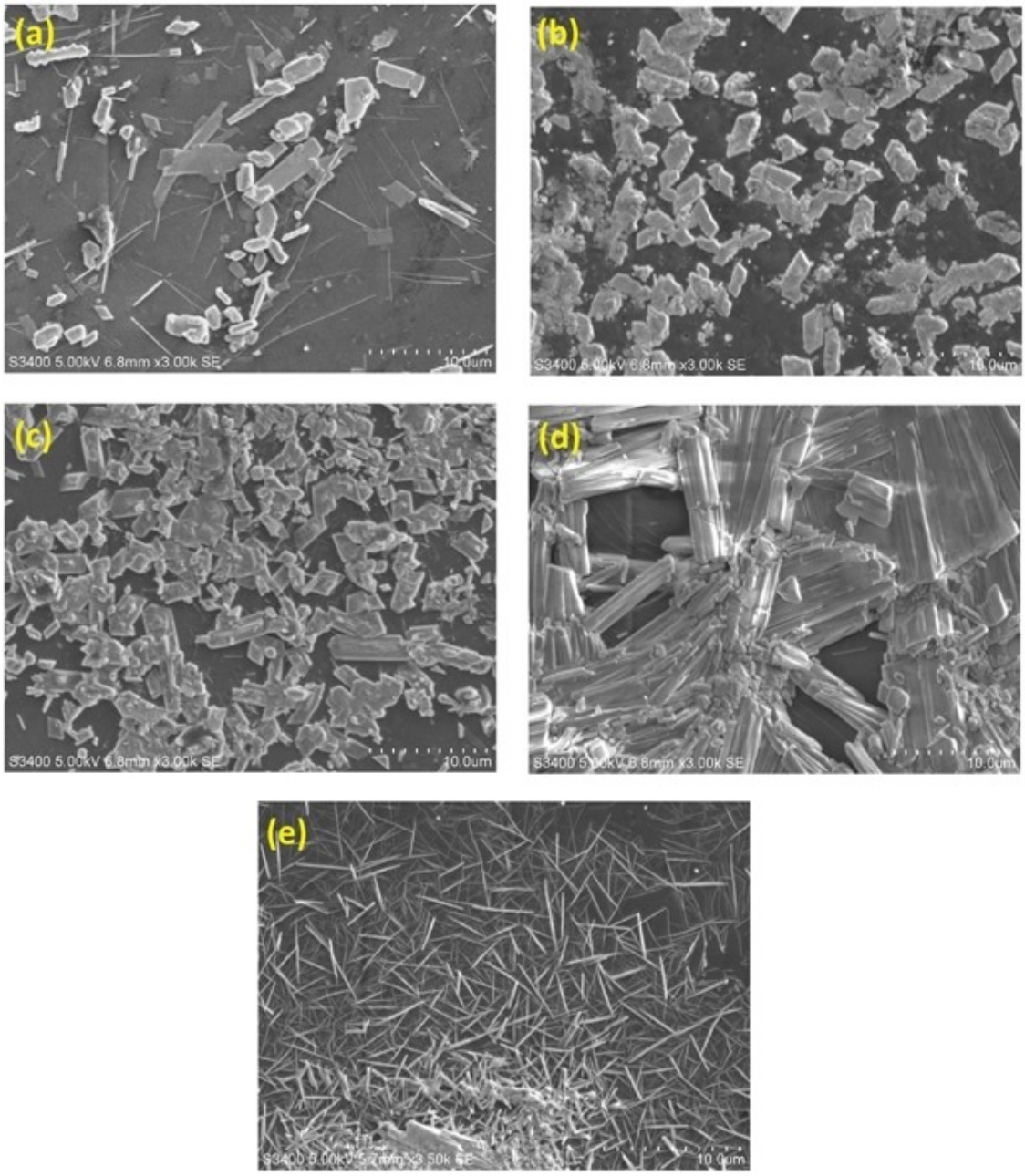

Figure 7. The SEM images of nanocomposites: (a) PMWAgP-1, (b) PMWAgP-2, (c) PMWAgP-3, (d) PMWAgP-4 and (e) PMWAgP-5.

the second set of redox peak, the conversion of emeraldine to the fully oxidized pernigraniline form is occurred.[46,47]

The CV curves with redox peaks are also due to the presence of MWCNTs–Ag composite. The redox peaks can be described by the following equation:

$$Ag_n^0 \rightleftharpoons Ag_n^+ + e^- \quad (1)$$

The MWCNTs–Ag counterpart contributed towards superior electrochemical behaviour by exhibiting rapid current response with cathodic and anodic current symmetry. This is mainly due to a good synergy between Ag nanoparticles and MWCNTs, which minimizes the internal resistance of MWCNTs–Ag composite and thus, provides more and more conductive pathways for electrolyte ions.

Similarly, the enhanced charge transfer in the developed PMWAgP could be of grain-to-grain wiring of the SPANI chains with uniformly distributed MWCNTs in the membrane. The presence of MWCNTs provides the conducting bridges between SPANI and these functions as electron tunnelling centers for the transfer of electrons from one polymer chain to the other. Also, the strong interactions between MWCNTs and SPANI, help to protect PANI chains from folding and thus provide a more exposed area of SPANI for redox reactions. It is also observed

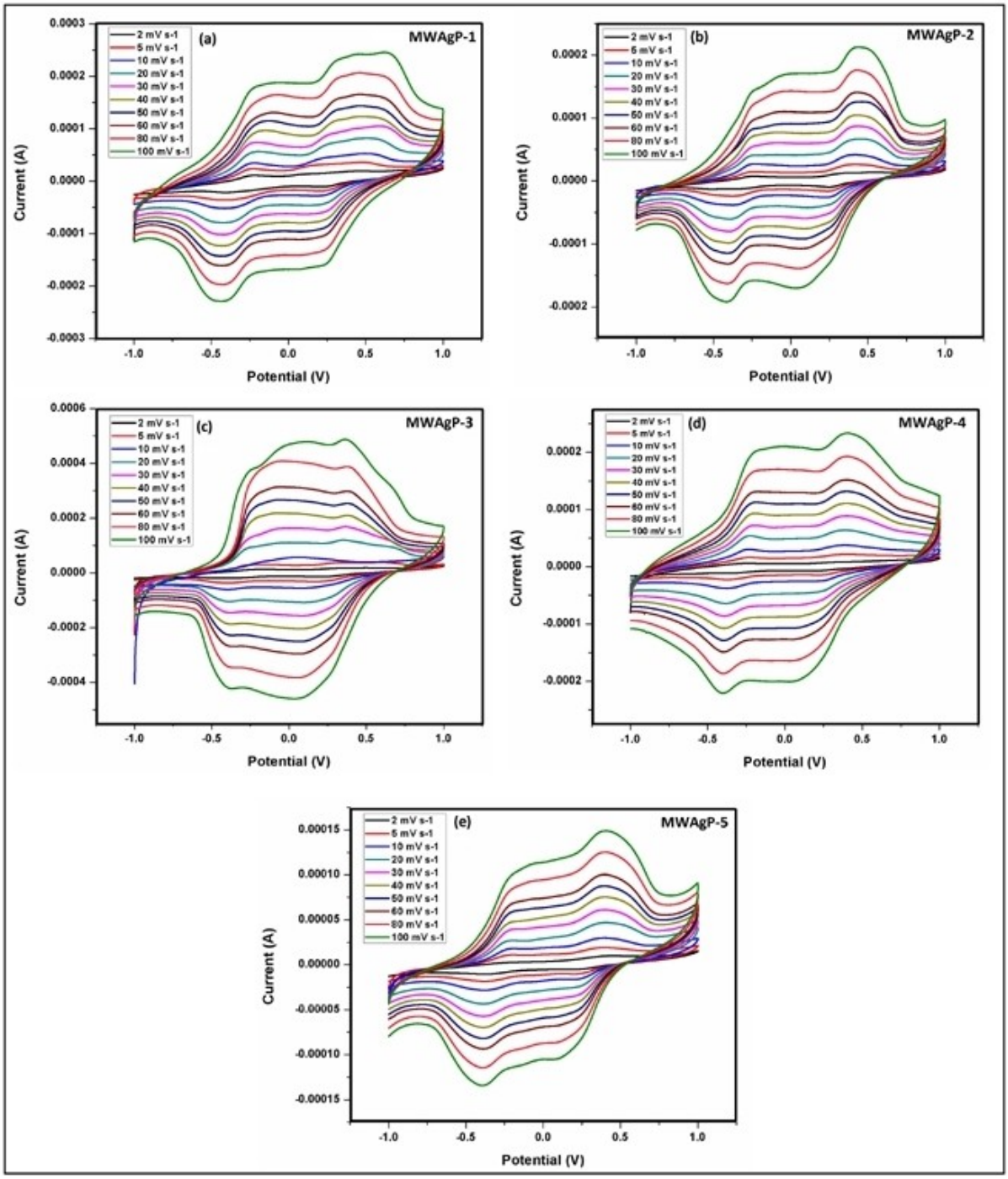

Figure 8. (a, b, c, d and e) Cyclic voltammograms of PMWAgP nanocomposites at different scan rates from 2 mV s^{-1} to 100 mV s^{-1}.

that the anodic and cathodic currents in the CV curves of PMWAgP nanocomposites (Figure 8) are almost equal. This could be due to the presence of MWCNTs in the matrix, which acts as the dopant for polyaniline and thereby stabilizes the system during the electrochemical study. This leads to the steady and reversible behavior of the composite.

From the CV curves, specific capacitance of the samples was calculated using Equation (2).

$$C_{sp} = \frac{\int Idv}{2m\Delta VS} \quad (2)$$

where, C_{sp} is the specific capacitance (F g^{-1}), $\int Idv$ is the area under the curve, m is the mass of electrode, S is the scan rate (mV s^{-1}) and $\triangle V$ is the potential window (V).

For all the five developed nanocomposites, the variation of specific capacitance values as a function of scan rate are plotted as shown in Figure 9b. From the plot, it is clear that the

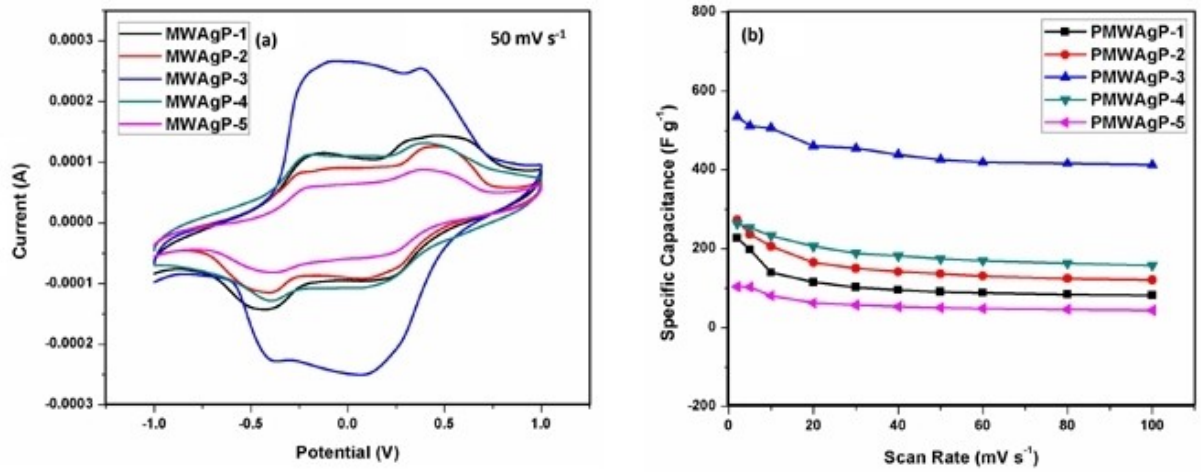

Figure 9. (a) The cyclic voltammograms of PMWAgP nanocomposites for the fixed scan rate of 50 mV s^{-1}, (b) the variation of specific capacitance of PMWAgP nanocomposites with the scan rate.

specific capacitance value is maximum for PMWAgP-3 nanocomposite. Besides, for all the nanocomposites, the specific capacitance was gradually decreased with increasing the scan rate. This is mainly due to inaccessibility of electrons in the electrode material at higher scan rates.[48] Understanding the superior electrochemical performance of PMWAgP-3 nanocomposite, the galvanostatic charge-discharge curves were recorded for the nanocomposite PMWAgP-3 at different current densities from 0.2 mA g^{-1} to 2.0 mA g^{-1} at a potential range of −1.0 V to + 1.0 V, which are presented in Figure 10a.

The curvature of the GCD curves indicates the pseudocapacitive behaviour of the electrode. The longest discharge time of the nanocomposite electrode demonstrates that the presence of MWCNTs and Ag doping was able to extend the duration of energy dissipation time owing to the presence of large interfacial area available for the Faradic reactions.[49] From the charge-discharge curves, again the specific capacitance (C_{sp}) of nanocomposite PMWAgP-3 was calculated using Equation (3):

$$Csp = \frac{2I(\Delta t)}{m(\Delta V)} \quad (3)$$

where, I is the discharge current (A), $\triangle$V is the potential window (V), m is the mass of the active material, and Δt is the discharge time (s).

The specific capacitance at the current density of 1 mA g^{-1} was found to be 572.8 F g^{-1}. The resulting specific capacitance is much superior to specific capacitance reported in our previous work.[50] The variation of specific capacitance to current density is shown in Figure 10b. Only 29.62 % capacitance loss was observed with increasing the current density from 0.2 to 2.0 mA g^{-1}, implying low electrode polarization. The enhanced specific capacitance value for PMWAgP-3 could be attributed to the EDLC characteristics of MWCNTs and the pseudocapacitive reactions from silver and polyaniline present in the nanocomposite. Initially, the electrochemical performance of PMWAgP electrode was increased with increasing the wt % of MW–Ag up to PMWAgP-3. This is because, as the wt % of MW–Ag nanohybrid increases, the nanohybrid facilitates much faster charge transport and thereby improves the electronic conductivity, and thus results in enhanced electrochemical performance. However, in the present study, the specific capacitance values decreased from PMWAgP-4 to PMWAgP-5 nanocomposites, and this could be due to the restacking of MW–Ag composite at the higher weight ratio of MW–Ag. The capacitance values obtained in this study are much higher than the previously reported MWCNT based ternary nanocomposites, like MWCNT-MnO_2-PANI electrodes (330 F g^{-1}),[51] MWCNT-PEDOT-PSS-MnO_2 nanocomposite electrodes (375 F g^{-1}),[52] MWCNTs-PANI-MnO_2 organic-inorganic hybrid nanoarchitecture (384 F g^{-1})[53] and MWCNT-PPy-PSS-MnO_2 nanocomposite electrodes (412 F g^{-1}).[54] To check the electrochemical stability of the electrode, the cycle-life study was also performed for the nanocomposite membrane PMWAgP-3 for 2500 cycles in 1 M H_2SO_4 electrolyte. The capacitance retention of the nanocomposite membrane as a function of the cycle number is shown in Figure 10c. It is observed that the PMWAgP-3 nanocomposite showed the specific capacitance retention of 83.5 % even after 2500 cycles. The resulting enhanced cycle-life stability of PMWAgP-3 nanocomposite could be due to sufficient accumulation of Ag at the surface of SPANI layers, which prevents the structural damage of PANI.

Electrochemical impedance spectroscopy (EIS) measurement has been considered as one of the principal methods to understand the basic behavior of supercapacitor electrode materials.[55,56] The EIS was adopted to evaluate the electrochemical frequency behavior of the developed electrodes in the electrolyte interface in the frequency range of 0.1–10^5 Hz with an AC perturbation of 5 mV. The Nyquist plot represents the imaginary component (Z′) against the real component (Z″) of the impedance. Generally, the Nyquist plot of a super-

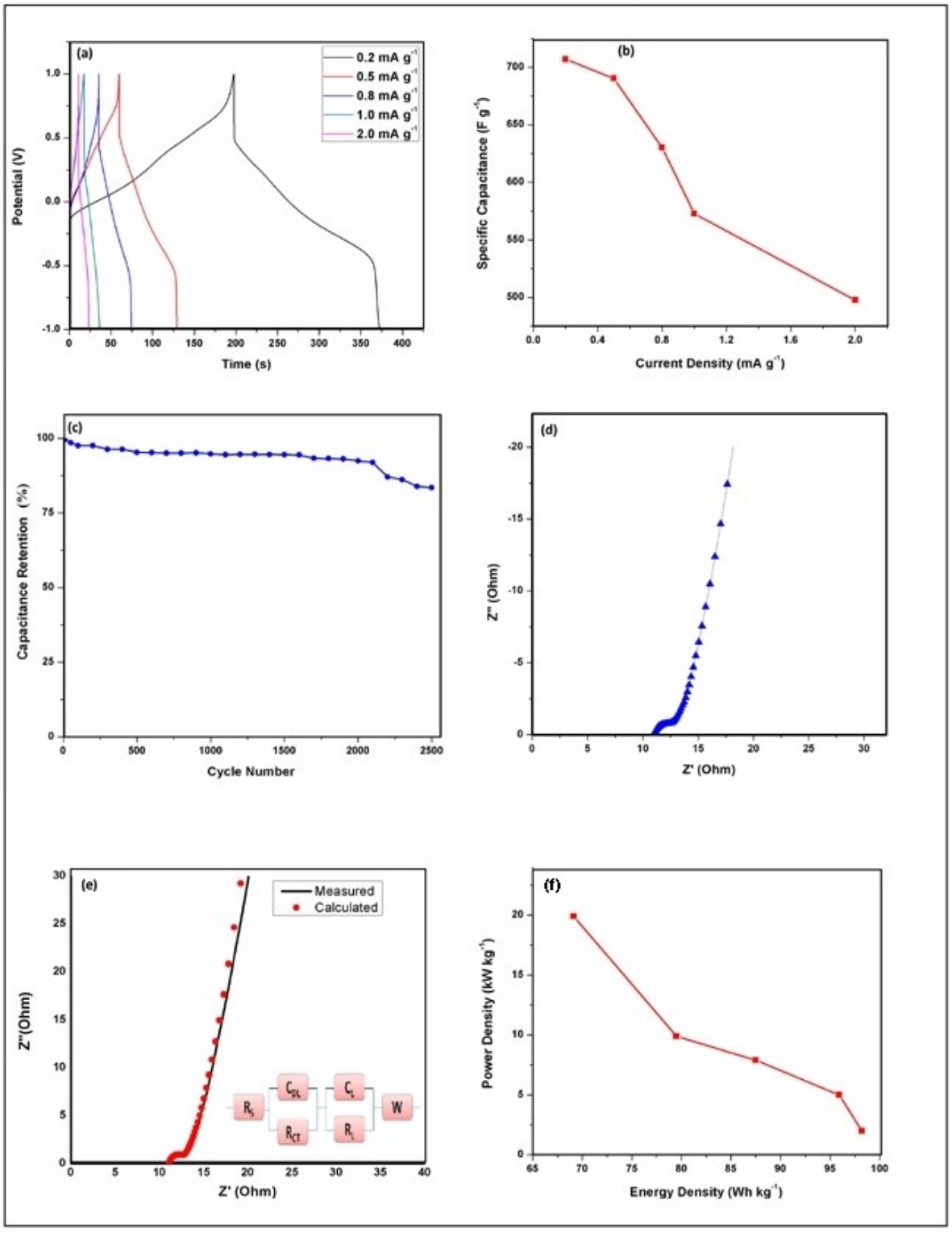

Figure 10. (a) The GCD curves of PMWAgP-3 nanocomposite at different current densities, (b) the variation of specific capacitance of PMWAgP-3 to current density, (c) the cycling performance of PMWAgP-3 nanocomposite membrane over 2500 charge-discharge cycles at current density of 1.0 mA g^{-1}, (d) the Nyquist plot of PMWAgP-3 nanocomposite electrode, (e) the Ragone plot of PMWAgP-3 nanocomposite showing good energy density and power density retention, and (f) the Nyquist plot of PMWAgP-3 in comparison with approximately matched circuit, inset figure shows the corresponding equivalent circuit.

capacitor exhibits a semicircle arch in the high-frequency region and a straight line at the low-frequency region. The resulting semicircle arch in the high-frequency region indicates the ion diffusion at the electrode-electrolyte interfaces.[57,58]

Figure 10d shows the Nyquist plot of impedance expressed a relatively linear response at lower frequencies and a semi-circle at higher frequencies. The higher frequency region indicates the resistance trend of the electrode under investigation.[59] The capacitive behavior of the system is evaluated from the straight line nearly parallel to the imaginary axis at the lower frequency region. The 45° portion of the plot corresponds to the porous structure of the electrode by the unique 3D architecture of the nanocomposite. This could enhance the electrochemical performance of the composites during the cycling processes. Besides, the imaginary part of the impedance curve approached a 90° vertical line is associated with a typical capacitive-type behavior of the developed nanocomposite. Figure 10e shows the Nyquist plot of PMWAgP-3 in comparison with approximately matched circuit. In the Nyquist plot, the small value of charge transfer resistance (R_{CT}, 1.26 Ω) is defined by the small arc, which supports for the strong synergistic effect between SPANI, Ag nanoparticles and MWCNTs. The presence of MWCNTs minimized the internal resistance of the nanocomposite by providing more and more conductive pathways for electrolyte ions. Inset of Figure 10e showed equivalent circuit, which consists of R_{CT} and C_{DL} in parallel connection and these are responsible for the small arc. The mass capacitance (C_L) in the parallel connection with leakage resistance (R_L) was responsible for the inclined behavior of the plot. The Warburg component (*W*) represented the shift from high frequency to low frequency.

To further evaluate the electrochemical behavior of the PMWAgP-3 nanocomposite electrode, we plotted the Ragone plot from the values of energy density (*E*) and power density (*P*) as shown in Figure 10f. Although CNT-based systems show extremely high power density, their energy density value is minimum. On the contrary, pseudocapacitive materials, such as conducting polymer-based systems, can show high energy density, but their power density is poor. However, from the plot it is observed that the ternary nanocomposite developed here demonstrated the highest energy density of 165.3 Wh kg^{-1}, at a power density of 9.3 W kg^{-1} and maintained energy density of 84.4 Wh kg^{-1} at a power density of 92.6 W kg^{-1}. The energy density value of the developed system is much superior to the values reported in the literature. For comparison, this value is higher than those of other MWCNT based supercapacitor electrode materials reported in literature, such as MWCNT/carbon nanosheets (41.3 Wh kg^{-1}),[60] (PANI/MWCNT) composite (7.03 Wh kg^{-1}),[26] AC/CNT/RGO (30 Wh kg^{-1}),[61] sGNS/cMWCNT/PANI (20.5 Wh kg^{-1}).[62] Moreover, developed nanocomposite showed much better performance than the commercially available activated carbon (3–5 Wh kg^{-1} energy density).[63] Based on the results, it is concluded that PMWAgP-3 nanocomposite provides high energy density and power delivery, and it therefore becomes a promising supercapacitor electrode material in the future.

These superior features of nanocomposite are attributed to the following factors: The observed enhanced electrochemical performance of nanocomposites is associated with the thin wrapping of sulfonated PANI over MWCNTs. The thin wrapping of polymer over the surface of MWCNTs increases the surface area of the polymer and thereby enhances the ions accessibility to most of the polymer chains. In conducting polymers, doping and dedoping create intercalation and depletion of ions in the polymer matrix to maintain the electroneutrality.[64] In the bulk polymer, due to low ionic diffusion, intercalation of ions into the innermost polymer chain is very difficult. However, the accessibility of ions to most of the polymer chains increased owing to the thin coating of conducting polymer over MWCNTs. Besides, the larger surface area of MWCNTs effectively shorten the travel distance for charge transport and thus provide the faster mass transfer of the electrolyte.[65] Thus, the prominent performance of the developed nanocomposite is associated with the optimal balance of high surface area resulted from MWCNTs–Ag content and the conducting sulfonated PANI. Furthermore, it might be due to uniformly dispersed sulfonated PANI in the crosslinked PVA matrix.

Electrochemical performance of the fabricated device

The newly designed and fabricated micro-supercapacitor device was subjected to cyclic voltammetry and galvanostatic charge-discharge technique to assess the electrochemical performance. The CV curves recorded for the fabricated device are shown in Figure 11a. The voltammograms clearly show that the fabricated supercapacitor device exhibited elliptical-shaped curves with no apparent redox peaks at all the scan rates, suggesting a typical EDLC behavior. Similarly, the galvanostatic charge-discharge (GCD) curves recorded in the potential range between +1 V and −1 V for different current densities from 2.0 to 5.0 mA g^{-1} as shown in Figure 11b illustrate a capacitive profile of a supercapacitor system. The triangular charge-discharge curves were found for the fabricated device. The specific capacitance of the fabricated micro-supercapacitor at a fixed current density of 5 mA g^{-1} was found to be 60.95 F g^{-1}.

The superior performance of the fabricated device is mainly due to a unique design employed for device fabrication. The inter-digital microelectrodes allow electrolyte ions to move in the horizontal direction, which reduces the ion diffusion pathway between the electrode material and electrolyte and this leads to instant charge storage. The fabricated micro-supercapacitors have several advantages. First, the travelling distance of the ions in the electrolyte can be easily controlled and shortened by eliminating the use of a separator. Second, having both electrodes in a single plane is compatible with on-chip integration.

Finally, the energy density and power density of the fabricated micro-supercapacitor device was calculated. The device exhibited an extremely high energy density of 8.46 Wh kg^{-1} with a power density of 67.81 W kg^{-1} at a current density of 5 mA g^{-1}. This infers that a significantly enhanced supercapacitor performance could be achieved through a unique design by choosing the ternary flexible electrode material judiciously. Also, this typical architecture has the potential to achieve high power density and energy density.

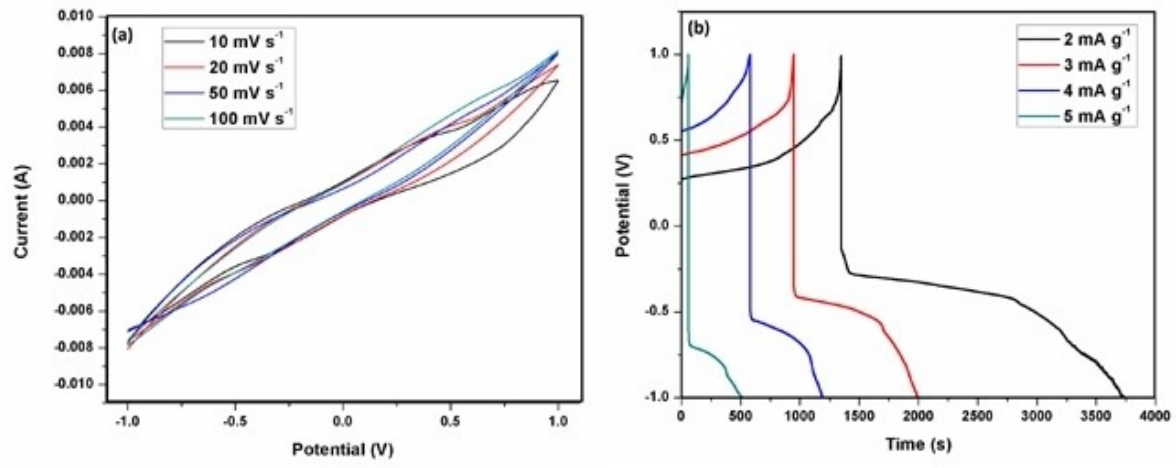

Figure 11. The electrochemical performance of supercapacitor device: (a) cyclic voltammograms of fabricated micro-supercapacitor at different scan rates, and (b) charge-discharge curves of micro-supercapacitor at different current densities.

Conclusions

A simple method was adopted to develop MWCNTs–Ag-SPANI ternary nanocomposites. The flexible membrane incorporated with ternary nanocomposite was developed using TEOS cross-linked PVA as a hybrid substrate. The optimized composite membrane exhibited an excellent thermal stability as evidenced by TGA and DSC results. The developed ternary nanocomposite membrane exhibited superior electrochemical performance with a specific capacitance of 572.8 F g^{-1} at 1 mA g^{-1} in 1 M H_2SO_4 electrolyte, having cycle-life stability of 83.5% even after 2500 cycles. The superior electrochemical performances have clearly suggested that the developed MWCNTs–Ag-SPANI ternary nanocomposite incorporated cross-linked PVA could be used as a good electrode material for supercapacitor. Considering the flexibility, high specific capacitance and good cycle-life stability of the developed membrane, flexible micro-supercapacitor device with a unique design was fabricated and investigated its performance systematically. The fabricated device exhibited a specific capacitance of 60.95 F g^{-1}, energy density of 7.46 Wh kg^{-1} and a power density of 67.81 W kg^{-1} at a current density of 5.0 mA g^{-1}. The significantly higher current density of the ternary nanocomposite membrane is associated with its higher electrical conductivity, fast ion transport and high surface area originated from the synergistic effect of MWCNTs, Ag and sulfonated PANI. Based on the superior electrochemical performance, the newly designed and fabricated micro-supercapacitor could be a promising device for supercapacitor applications.

Supporting Information Summary

The details on experimental methods including synthesis of nanocomposite membranes and fabrication of micro-supercapacitor device, physico-chemical characterizations and electrochemical measurements are provided in supporting information.

Acknowledgements

Authors (Dr. Satishkumar R. Naik and Dr. Balappa B. Munavalli) sincerely thank the UGC, New Delhi, for awarding the RFSMS fellowships to undertake the research. The authors acknowledge the financial support extended by the Department of Science & Technology, New Delhi under DST-PURSE-Phase-II Program [Grant No. SR/PURSE PHASE-2/13(G)]. This work is also supported by the UGC, New Delhi under CPEPA Program [Grant No. 8-2/2008(NS/PE)].

Conflict of Interest

The authors declare no conflict of interest.

Keywords: conducting materials · membranes · micro-supercapacitor device · specific capacitance · ternary nanocomposite

[1] M. Winter, R. J. Brodd, *Chem. Rev.* **2004**, *104*, 4245–4269.
[2] C. Liu, F. Li, L. P. Ma, H. M. Cheng, *Adv. Mater.* **2010**, *22*, E28-62.
[3] M. Jayalakshmi, K. Balasubramanian, *Int. J. Electrochem. Sci.* **2008**, *3*, 1196–1217.
[4] A. I. Torvi, S. R. Naik, M. Y. Kariduraganavar, *Chemical Data Collection* **2018**, *17–18*, 459–471.
[5] P. Simon, Y. Gogotsi, *Nat. Mater.* **2008**, *7*, 845–854.
[6] V. L. Pushparaj, M. M. Shaijumon, A. Kumar, S. Murugesan, L. Ci, R. Vajtai, R. J. Linhardt, O. Nalamasu, P. M. Ajayan, *Proc. Natl. Acad. Sci. USA* **2007**, *104*, 13574–13577.
[7] S. R. Naik, A. I. Torvi, D. D. Achari, M. Y. Kariduraganavar, *New J. Chem.* **2019**, *43*, 16017–16032.
[8] Y. Li, X. Yan, X. Zheng, H. Si, M. Li, Y. Liu, Y. Sun, Y. Jianga, Y. Zhang, *J. Mater. Chem. A* **2016**, *4*, 17704–17710.
[9] Y. Shi, L. Pan, B. Liu, Y. Wang, Y. Cui, Z. Bao, G. Yu, ***J. Mater. Chem. A*** **2014**, ***2***, 6086–6091.
[10] M. S. Javed, M. Wang, D. Guo, L. Chen, X. Wang, C. Hu, Yi Xi, *J. Power Sources* **2015**, *285*, 63–69.
[11] X. Li, Y. Tang, J. Song, W. Yang, M. Wang, C. Zhu, W. Zhao, J. Zheng, Y. Lin, *Carbon* **2018**, *129*, 236–244.
[12] S. Luo, J. Zhao, J. Zou, Z. He, C. Xu, F. Liu, Y. Huang, L. Dong, L. Wang, H. Zhang, *ACS Appl. Mater. Interfaces* **2018**, *10*, 3538–3548.

[13] J. P. C. Trigueiro, R. L. Lavall, G. G. Silva, *Electrochim. Acta* **2016**, *187*, 312–322.
[14] V. H. R. de Souza, M. M. Oliveira, A. J. G. Zarbin, *J. Power Sources* **2014**, *260*, 34–42.
[15] L. L. Zhang, X. S. Zhao, *Chem. Soc. Rev.* **2009**, *38*, 2520–2531.
[16] B. Andrew, *J. Power Sources* **2000**, *91*, 37–50.
[17] Y. Gogotsi, P. Simon, *Science* **2011**, *334*, 917–918.
[18] X. Zhao, B. M. Sanchez, P. J. Dobson, P. S. Grant, *Nanoscale* **2011**, *3*, 839–855.
[19] Z. Niu, W. Zhou, J. Chen, G. Feng, H. Li, W. Ma, J. Li, H. Dong, Y. Ren, D. Zhao, S. Xie, *Energy Environ. Sci.* **2011**, *4*, 1440–1446.
[20] C. Peng, S. Zhang, D. Jewell, G. Z. Chen, *Prog. Nat. Sci.* **2008**, *18*, 777–788.
[21] Y. Zhai, Y. Dou, D. Zhao, P. F. Fulvio, R. T. Mayes, S. Dai, *Adv. Mater.* **2011**, *23*, 4828–4850.
[22] V. Gupta, N. Miura, *Electrochim. Acta* **2006**, *52*, 1721–1726.
[23] N. Gull, S. M. Khan, A. Islam, S. Zia, M. Shafiq, A. Sabir, M. A. Munawar, M. T. Z. Butt, T. Jamil, *Mater. Chem. Phys.* **2016**, *172*, 39–46.
[24] Y. Zhou, Z.-Y. Qin, L. Li, Y. Zhang, Y.-L. Wei, L.-F. Wang, M.-F. Zhu, *Electrochim. Acta* **2010**, *55*, 3904–3908.
[25] C. Meng, C. Liu, S. Fan, *Electrochem. Commun.* **2009**, *11*, 186–189.
[26] G. Otrokhov, D. Pankratov, G. Shumakovich, M. Khlupova, Y. Zeifman, I. Vasil'eva, O. Morozova, A. Yaropolov, *Electrochim. Acta* **2014**, *123*, 151–157.
[27] Z.-Z. Zhu, G.-C. Wang, M.-Q. Sun, X.-W. Li, C.-Z. Li, *Electrochim. Acta* **2011**, *56*, 1366–1372.
[28] M. R. Z. Karim, K. T. Lim, C. J. Lee, M. T. I. Bhuiyan, H. J. Kim, L.-S. Park, M. S. Lee, *J. Polym. Sci., Part A-1: Polym. Chem.* **2007**, *45*, 5741–5747.
[29] Q. Jia, S. Shan, L. Jiang, Y. Wang, D. Li, *J. Appl. Polym. Sci.* **2012**, *125*, 3560–3566.
[30] V. K. Rangari, G. M. Mohammad, S. Jeelani, A. Hundley, K. Vig, S. R. Singh, S. Pillai, *Nanotechnology* **2010**, *21*, 095102 (1-11).
[31] H. Yun, J. D. Kim, H. C. Choi, C. W. Lee, *Bull. Korean Chem. Soc.* **2013**, *34*, 3261–3264.
[32] R. Paul, A. Maity, A. Mitra, P. Kumbhakar, A. K. Mitra, *J. Nanopart. Res.* **2011**, *13*, 5749–5757.
[33] D. S. Patil, J. S. Shaikh, D. S. Dalavi, S. S. Kalagi, P. S. Patil, *Mater. Chem. Phys.* **2011**, *128*, 449–455.
[34] M. A. F. Robertson, K. A. Mauritz, *J. Polym. Sci. Part B* **1998**, *36*, 595–606.
[35] D. P. Dubal, R. Holze, *New J. Chem.* **2013**, *37*, 403–408.
[36] B. R. Sankapal, H. B. Gajare, D. P. Dubal, R. B. Gore, R. R. Salunkhe, H. Ahn, *Chem. Eng. J.* **2014**, *247*, 103–110.
[37] K. R. Reddy, K.-P. Lee, J. Y. Kim, Y. Lee, *J. Nanosci. Nanotechnology* **2008**, *8*, 5632–5639.
[38] K. R. Reddy, K. P. Lee, A. I. Gopalan, *Colloids and Surfaces A: Physicochem. Eng. Aspects* **2008**, *320*, 49–56.
[39] Y. Ding, Y. Wang, L. Su, H. Zhang, Y. Lei, *J. Mater. Chem.* **2010**, *20*, 9918–9926.
[40] T. Alammar, A.-V. Mudring, *J. Mater. Sci.* **2009**, *44*, 3218–3222.
[41] Y. Lu, Y. Wang, W. Chen, *J. Power Sources* **2011**, *196*, 3033–3038.
[42] A. M. Sajjan, B. K. Jeevan Kumar, A. A. Kittur, M. Y. Kariduraganavar, *J. Ind. Eng. Chem.* **2013**, *19*, 427–437.
[43] J. Zhu, S. Wei, L. Zhang, Y. Mao, J. Ryu, A. B. Karki, D. P. Young, Z. Guo, *J. Mater. Chem.* **2011**, *21*, 342–348.
[44] Z. Xu, T. Wu, J. Shi, K. Teng, W. Wang, M. Ma, J. Li, X. Qian, C. Li, J. Fan, *J. Membr. Sci.* **2016**, *520*, 281–293.
[45] Q. Fu, F. Tietz, D. Stöver, *J. Electrochem. Soc.* **2006**, *153*, D74-D83.
[46] Y. Li, X. Zhao, Q. Xu, Q. Zhang, D. Chen, *Langmuir* **2011**, *27*, 6458–6463.
[47] H. Fei, N. Saha, N. Kazantseva, T. Babkova, M. Machovsky, G. Wang, H. Bao, P. Saha, *J. Mater. Sci. Mater. Electron.* **2018**, *29*, 3025–3034.
[48] W. Liu, X. Yan, J. Lang, C. Peng, Q. Xue, *J. Mater. Chem.* **2012**, *22*, 17245–17253.
[49] C. He, S. Sun, H. Peng, C. P. Tsui, D. Shi, X. Xie, Y. Yang, *Compos. B. Eng.* **2016**, *106*, 81–87.
[50] A. I. Torvi, B. B. Munavalli, S. R. Naik, M. Y. Kariduraganavar, *Electrochim. Acta* **2018**, *282*, 469–479
[51] Q. Li, J. Liu, J. Zou, A. Chundec, Y. Cheb, L. Zhai, *J. Power Sources* **2011**, *196*, 565–572.
[52] R. K. Sharma, L. Zhai, *Electrochim. Acta* **2009**, *54*, 7148–7155.
[53] C. Z. Yuan, L. H. Su, B. Gao, X. G. Zhang, *Electrochim. Acta* **2008**, *53*, 7039–7047.
[54] R. K. Sharma, A. Karakoti, S. Seal, L. Zhai, *J. Power Sources* **2010**, *195*, 1256–1262.
[55] M. Jana, S. Saha, P. Samanta, N. C. Murmu, N. H. Kim, T. Kuila, J. H. Lee, *Nanotechnology* **2015**, *26*, 075402.
[56] N. Zhu, W. Liu, M. Xue, Z. Xie, D. Zhao, M. Zhang, J. Chen, T. Cao, *Electrochim. Acta* **2010**, *55*, 5813–5818.
[57] J. Song, M. Z. Bazant, *J. Electrochem. Soc.* **2013**, *160*, A15-A24.
[58] D. Antiohos, K. Pingmuang, M. Romano, S. Beirne, T. Romeo, P. Aitchison, A. Minett, G. Wallace, S. Phanichphant, J. Chen, *Electrochim. Acta* **2013**, *101*, 99–108
[59] Y.-K. Zhou, B.-L. He, W.-J. Zhou, J. Huang, X.-H. Li, B. Wu, H.-L. Li, *Electrochim. Acta* **2004**, *49*, 257–262.
[60] J. P. C. Trigueiro, R. L. Lavall, G. G. Silva, *Electrochim. Acta* **2016**, *187*, 312–322.
[61] X. Li, Y. Tang, J. Song, W. Yang, M. Wang, C. Zhu, W. Zhao, J. Zheng, Y. Lin, *Carbon* **2018**, *129*, 236–244.
[62] J. Shen, C. Yang, X. Li, G. Wang, *ACS Appl. Mater. Interfaces* **2013**, *5*, 8467–8476.
[63] H.-C. Tao, S.-C. Zhu, X.-L. Yang, L.-L. Zhang, S.-B. Ni, *Electrochim. Acta* **2016**, *190*, 168–177.
[64] A. Rudge, I. Raistrick, S. Gottesfeld, J. P. Ferraris, *Electrochim. Acta* **1994**, *39*, 273–287.
[65] Z.-S. Wu, Y. Sun, Y.-Z. Tan, S. Yang, X. Feng, K. Müllen, *J. Am. Chem. Soc.* **2012**, *134*, 19532–19535.

Submitted: September 2, 2020
Accepted: March 16, 2021

FULL PAPERS

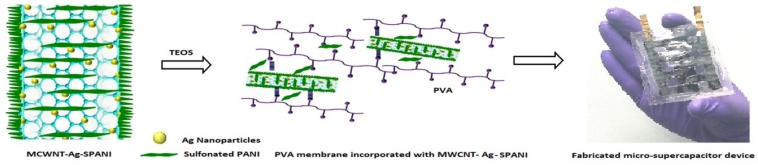

*Dr. S. R. Naik, Dr. A. I. Torvi, Dr. B. B. Munavalli, Dr. D. D. Achari, Prof. M. Y. Kariduraganavar**

Synthesized MWCNTs–Ag-SPANI ternary nanocomposite and incorporated into the PVA matrix to develop the flexible nanocomposite membrane. Based on the superior electrochemical performance exhibited by the developed ternary nanocomposite membrane, fabricated the micro-supercapacitor device and evaluated the electrochemical performance. The fabricated micro-supercapacitor device exhibited the specific capacitance of 60.95 F g^{-1}, energy density of 7.46 Wh kg^{-1} and power density of 67.81 W kg^{-1} at a current density of 5.0 mA g^{-1}.

Author Contributions

S.N. Data curation:Lead; Formal analysis:Lead; Investigation:Lead; Methodology:Lead; Writing – original draft:Lead; Writing – review & editing:Lead
A.T. Visualization:Supporting
B.M. Validation:Supporting
D.A. Data curation:Supporting; Investigation:Supporting